Coexistence of ferromagnetic and antiferromagnetic phases in Nd$_{0.5}$Ca$_x$Sr$_{0.5-x}$MnO$_3$ manganites

Coexistence of ferromagnetic and antiferromagnetic phases in $Nd_{0.5}Ca_xSr_{0.5-x}MnO_3$ manganites

S Savitha Pillai[1], G Rangarajan[1], N P Raju[2], A J Epstein[2] and P N Santhosh[1]

[1] Low Temperature Physics Laboratory, Department of Physics, Indian Institute of Technology Madras, Chennai 600036, India
[2] Department of Physics, Ohio State University, Columbus, OH 43210, USA

E-mail: santhosh@physics.iitm.ac.in

Abstract

We have investigated the spontaneous magnetization exhibited in $Nd_{0.5}Ca_xSr_{0.5-x}MnO_3$ ($x = 0.1, 0.2, 0.3$ and 0.4) (NCSMO) samples by measurements of magnetization and electron spin resonance. As like end members, the samples crystallize in an orthorhombic structure with *Imma* ($x = 0.1$) and *Pnma* ($0.2, 0.3$ and 0.4) space groups. Transport studies reveal that Mott small polaron hopping type conduction occurs in the insulating regime of the samples. The drop in the zero field cooled dc magnetization, a large thermal irreversibility of the field cooled and zero field cooled data and the presence of two resonance fields below the temperature T^* strongly suggest the coexistence of phases in NCSMO. The occurrence of coexisting phases may be strongly influenced by the random distribution of A-site cations such as Sr and Ca, which in turn leads to delocalization of e_g electrons and real space ordering of Mn^{3+} and Mn^{4+} ions.

1. Introduction

Interest in manganites continues due to their complex magnetotransport properties and phase transition phenomena [1]. Among the manganites $A_{1-x}A'_xMnO_3$ with $x = 0.5$ have been extensively studied due to their charge, orbital and spin ordering properties [2, 3]. $Nd_{0.5}Ca_{0.5}MnO_3$ (NCMO) and $Nd_{0.5}Sr_{0.5}MnO_3$ (NSMO) are examples of such systems, which show phase competition between the ferromagnetic metallic and the charge-orbital ordered antiferromagnetic states. NSMO undergoes a ferromagnetic transition near 250 K followed by a CE-type antiferromagnetic phase near 160 K and charge ordering takes place at a temperature which coincides with the Néel temperature [3, 4]. Unlike NSMO, in NCMO charge ordering occurs at 250 K followed at 150 K by an A-type antiferromagnetic transition. The charge-ordered antiferromagnetic state in half-doped manganites can be understood within the

Goodenough model (GM) [5]. According to GM, superexchange interaction between orbital of the charge-ordered Mn^{3+}/Mn^{4+} system leads to the AFM state. Recent results based on the Hubbard model reveal that on-site and nearest-neighbor Coulomb repulsion leads to charge ordering in manganites [6].

The Mn^{3+}/Mn^{4+} ratio is one of the parameters that can effectively control the different interactions such as double-exchange [7], superexchange and Coulomb interaction among Mn ions, and it can modify the magnetotransport properties of manganites. Depending on the relative ratio of Mn^{3+} and Mn^{4+} there is competition between double exchange ferromagnetism (FM) and superexchange antiferromagnetism (AFM) resulting in a homogeneous or inhomogeneous distribution of electron density which in turn leads to a complex series of phase transitions [3, 8–10] and the coexistence different magnetic phases in manganites [8–10]. The average size of the A-site cation is another important parameter that can influence the magnetic and electrical characteristics of the material. The relative ease with which the perovskite structure incorporates the different sized A-site cations makes it easier to design a variety of manganites exhibiting a wide range of magnetic and electrical characteristics. With different sized ions occupying the A-site, there will be a size disorder among the ions occupying the A-site. The importance of A-site disorder (variance σ^2) for the magnetic and electrical transitions is well understood by now [39]. Recent high resolution synchrotron x-ray diffraction [3], neutron diffraction [3, 12], electron spin resonance (ESR) [13, 14], nuclear magnetic resonance (NMR) [15, 16] and magnetic studies [12, 16] reveal the coexistence of different phases in the manganites. But it is still not very clear whether the phase separation phenomenon is due to inhomogeneous distribution of different A-site ions or to crystallographic or magnetic interactions.

NCMO and NSMO are charge-ordered insulators and the solid solutions of these end members, NCSMO ($Nd_{0.5}Ca_xSr_{0.5-x}MnO_3$), have been reported to show interesting magnetic and electrical properties [17]. As in charge-ordered systems the ratio of Mn^{3+} to Mn^{4+} is 1:1 for NCSMO; however it has been reported that due to the disorder in the A-site cation radius ($\langle r_A \rangle$), the CO state collapses and became ferromagnetic metallic in the ground state [17, 18]. Re-entrant ferromagnetism was invoked to represent these compositions. We have performed x-ray diffraction (XRD), resistivity, magnetization and ESR studies to understand the re-entrant phenomenon in NCSMO and the experimental results indicate the coexisting phases in NCSMO.

2. Experimental details

$Nd_{0.5}Ca_xSr_{0.5-x}MnO_3$ ($x = 0.1, 0.2, 0.3$ and 0.4) was prepared by the citrate gel method. As this method is known to give a high degree of homogeneity, we employed this to rule out the extrinsic factors that can lead to phase separation behavior. The starting materials, Nd_2O_3, $SrCO_3$ and $CaCO_3$, were first dissolved in dilute nitric acid, $Mn(CH_3COO)_2 \cdot 4H_2O$ in water and then an appropriate mixture of citric acid. The resulting gel was decomposed at $300\,°C$ and the acquired precursor powder was heated in air at $600\,°C$ for 6 h and then at $1100\,°C$ for 24 h to improve crystallinity. Later the powder was pelletized and sintered at $1300\,°C$ for 12 h. Powder XRD patterns of the samples were recorded using a PANalytical X'pertPro diffractometer with step size of 0.004, with Cu Kα radiation. A Ni filter was used to block the K_β radiation. We used a programmable divergence slit ($1/2°$) in the fixed slit mode to collect the data for Rietveld analysis. XRD data for the samples were analyzed with the Rietveld technique using the program GSAS. We used a shifted Chebyshev polynomial with 10 variables to fit the background. Resistivity measurement was performed using the conventional four-probe method in the temperature range 35–300 K. DC magnetization measurements were

Table 1. Structural parameters of $Nd_{0.5}Ca_xSr_{0.5-x}MnO_3$ (NCSMO).

NCSMO	$x = 0.1$	$x = 0.2$	$x = 0.3$	$x = 0.4$
2θ range (deg)	10–90	10–90	10–90	10–90
σ^2	0.005 01	0.004 29	0.003 22	0.001 82
Space group	*Imma*	*Pnma*	*Pnma*	*Pnma*
a (Å)	5.4217(2)	5.4172(5)	5.4163(7)	5.4036(1)
b (Å)	7.6363(3)	7.6395(7)	7.6388(9)	7.6267(1)
c (Å)	5.4556(2)	5.4092(5)	5.4090(1)	5.3982(1)
Volume (Å^3)	225.87(3)	223.858(8)	223.792(3)	222.472(9)
Nd/Sr/Ca x	0	0.018 36(2)	0.0165(3)	0.0212(2)
Nd/Sr/Ca y	0.25	0.25	0.25	0.25
Nd/Sr/Ca z	−0.0087(3)	−0.0155(4)	−0.0192(2)	−0.0145(2)
Uiso (Å^2)	0.0154(3)	0.0246(1)	0.0249(3)	0.0226(2)
Mn x	0	0	0	0
Mn y	0	0	0	0
Mn z	0.5	0.5	0.5	0.5
Uiso (Å^2)	0.002 37(5)	−0.0133(5)	−0.0242(5)	−0.0122(5)
O_{AX} x	0	0.002(1)	0.0093(2)	−0.007(1)
O_{AX} y	0.25	0.25	0.25	0.25
O_{AX} z	0.493(4)	0.485(4)	0.489(2)	0.484(6)
Uiso (Å^2)	0.0249(2)	−0.016(2)	−0.037(3)	0.052(2)
O_{EQ} x	0.75	0.6978(1)	0.685(1)	0.690(2)
O_{EQ} y	0.024(1)	0.0245(2)	0.0308(9)	0.027(1)
O_{EQ} z	0.25	0.3017(2)	0.309(1)	0.323(2)
Uiso (Å^2)	0.0161(2)	0.028(2)	0.0206(2)	0.028(3)
Mn–O$_1$	2*1.9094(5)	2*1.9117(9)	2*1.911(5)	2*1.909(1)
Mn–O$_2$	4*1.9320(9)	2*1.966(1)	2*1.968(8)	2*2.022(9)
		2*1.961(9)	2*2.005(9)	2*1.959(9)
Mn–O–Mn	173.4(7)	164.55(2)	162.15(9)	160.5 (5)
$\langle w \rangle$	6.6	15.45	17.85	19.5
R_{WP}	6.95%	7.56%	6.96%	6.74%
R_P	5.47%	5.93%	5.5%	5.31%
$R(F^2)$	8%	10.99%	9.64%	7.97%

carried out using a superconducting quantum interference device (SQUID) magnetometer in the temperature range 4.2–300 K and a magnetic field of 50 Oe. The ESR measurements were performed with a Varian E-112 continuous-wave spectrometer at X-band frequency ($\approx$9.35 GHz). Approximately 0.03 g of fine powder was used for the measurement.

3. Results and discussions

Rietveld analysis of the XRD data shows that the samples were all single phase with an orthorhombic perovskite structure. Rietveld analysis of samples were carried out by using structural parameters of the parent compounds NCMO (*Pnma*) and NSMO (*Imma*) as starting values [11]. It is found that NCSMO with a composition $x = 0.1$ crystallizes with the *Imma* space group whereas all other compositions give best fit with the *Pnma* space group. The refined structural parameters at room temperature are given in table 1. The values of the lattice parameters of the composition $x = 0.2$ and 0.3 are almost similar whereas the end compositions show a substantial difference. The values of b/c are found to be less than $\sqrt{2}$, which shows that the distortion is mainly driven by a cooperative Jahn–Teller effect [19]. The bond angles
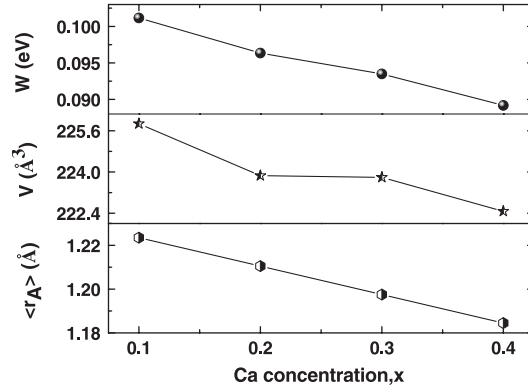
3

Figure 1. The average radius of the A-site cation ($\langle r_A \rangle$), lattice volume (V) and bandwidth (W) as a function of Ca concentration, x, of the samples.

and bond lengths indicate that the tilt of MnO_6 octahedra increases with an increase in Ca concentration which in turn increases the canting moment [12]. Moreover the value of the electronic bandwidth W, which depends on the $\langle Mn-O-Mn \rangle$ angle and $d_{\langle Mn-O \rangle}$ through the relation

$$W \alpha \cos \omega / d_{\langle Mn-O \rangle}^{3.5}, \qquad \text{where } \omega = 1/2(\pi - \langle Mn-O-Mn \rangle),$$

also has a substantial effect on the properties of the manganites [20]. The wide bandwidth enhances the overlap between the ions which increases the hopping rate of e_g carriers, favors the double exchange interaction (DE) between the carriers and results in on-site ferromagnetic coupling between the Mn sites and suppresses antiferromagnetic ordering [20, 21]. The competition between the ferromagnetic DE and antiferromagnetic interactions is very sensitive to W; a small change in W has profound effect on the transport as well as magnetic properties of manganites [20]. The value of W is found to decrease with x so that the ferromagnetic DE interactions weaken with x. The metal–insulator transition of NCSMO with $x = 0.1$, 0.2 and 0.3 is attributed to a relatively large electronic bandwidth compared to $x = 0.4$, which can be seen in the figure 1. As in end-members, the narrow bandwidth W leads to the localization of charge carriers, resulting in an insulating nature of NCSMO 0.4 [11]. The variations of the average radius of the A-site cation $\langle r_A \rangle$ and the cell volume (V) with Ca concentration (x) are also plotted in figure 1. The local lattice distortions arising due to the size mismatch of A-site cations lead to competition between an AFM superexchange and FM interaction between Mn ions in half-doped NCSMO [12].

Figure 2(a) shows the temperature dependence of resistivity of the samples. Unlike the parent compounds, the compositions $x = 0.1$, 0.2 and 0.3 show a distinct metal–insulator transition (MI) with peak temperatures of 162 K, 150 K, and 140 K, respectively. The MI transition in NCSMO ($x = 0.1$, 0.2 and 0.3) indicates the collapse of charge ordering due to the random distributions of A-site cations, which disturbs the regular arrangements of Mn^{3+} and Mn^{4+} ions and favors ferromagnetic interactions. However, the $x = 0.4$ composition shows an insulating behavior similar to NCMO. In analogy to doped manganites, we have used the Mott small polaron hopping model to fit the insulating region of the transport properties of NCSMO (figure 2(b)). In a small polaron system, electronic transport occurs due to the hopping of electrons and associated distortion into an adjacent site by overcoming the energy barrier. The resistivity in the small polaron model can be expressed by the general form [22]

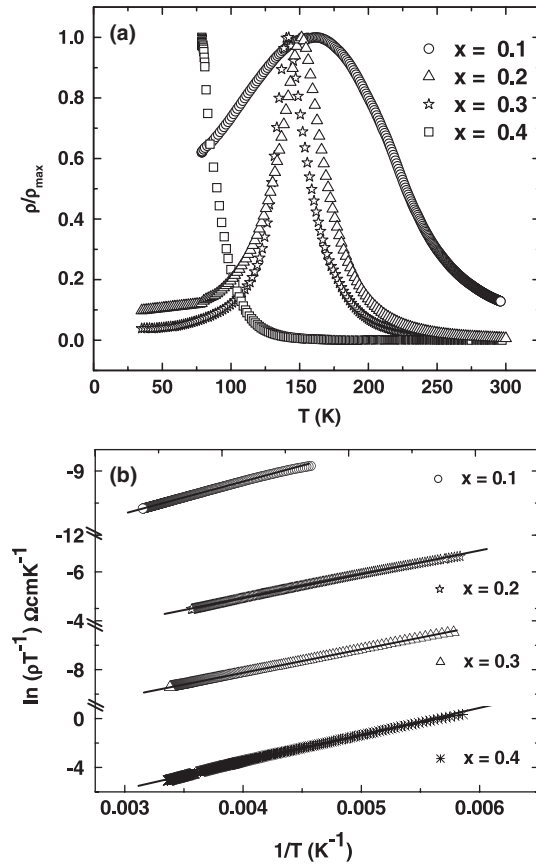$$\rho_{(T)} = \rho_{(0)} T e^{(E_a / k_B T)},$$

Figure 2. (a) The temperature dependence of resistivity of NCSMO ($x = 0.1$, 0.2, 0.3 and 0.4). (b) The small polaron hopping model fits to the insulating regime of the resistivity data of NCSMO.

Table 2. Activation energies for the samples $Nd_{0.5}Ca_xSr_{0.5-x}MnO_3$ from resistivity fit (E_a) and ESR intensity (ΔE). T^*, T_C and the effective magnetic moment are calculated from the Curie–Weiss fit.

NCSMO	E_a (eV)	ΔE (eV)	T^* (K)	T_C (K)	μ_{eff} (μ_B)
$x = 0.1$	0.138	0.054	225	215	6.17
$x = 0.2$	0.168	0.041	185	145	6.68
$x = 0.3$	0.165	0.047	170	130	6.83
$x = 0.4$	0.180	0.059	140	80	6.54

where $\rho_{(0)}$ is a temperature independent term, which signifies polaron-mediated transport at high temperature in NCSMO. The calculated values of activation energy (E_a) lie between 0.138 and 0.18 eV (table 2). These values are found to be high compared with those for the ground state ferromagnetic $Nd_{0.67}Sr_{0.33}MnO_3$($E_a = 0.1$ eV), $La_{0.67}Ca_{0.33}MnO_3$($E_a = 0.086$ eV) etc [23] and low compared to antiferromagnetic $NdMnO_3$ ($E_a = 0.3$ eV) [24]. The values of E_a indicate that the localization of polarons is more for the composition 0.4 which is reflected in the absence of a metal–insulator transition in NCSMO 0.4 [25].

Figure 3 shows the temperature dependence of dc magnetization for NCSMO in zero field cooled (ZFC) and field cooled (FC) conditions at a field of 50 Oe. The value of T_C, defined
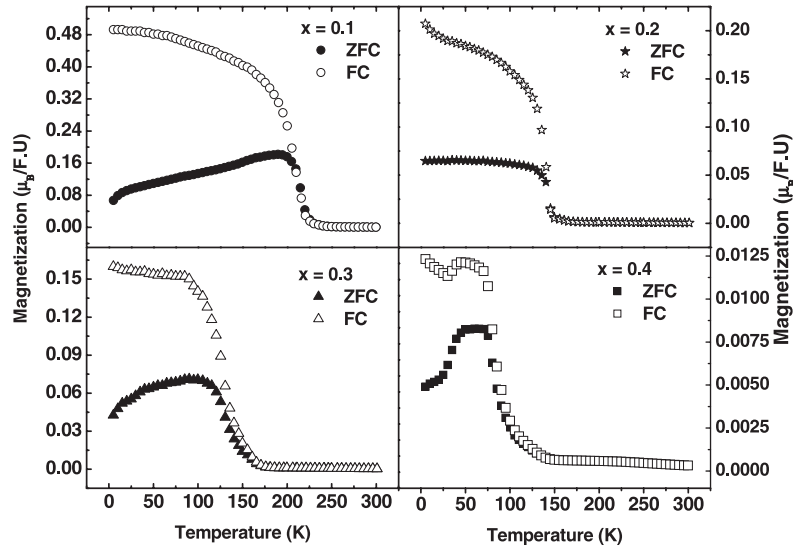
Figure 3. FC and ZFC magnetization of $Nd_{0.5}Ca_xSr_{0.5-x}MnO_3$.

as the temperature of the maximum slope in dM/dT, decreases with an increase in the Ca concentration and this is ascribed to a narrowing of the bandwidth with decrease in the average radius [26]. All the samples show thermal irreversibility in the ZFC and FC magnetization data. The large difference between M_{FC} and M_{ZFC} data suggests an inhomogeneous mixture of a FM and AFM nature rather than a distinct FM or AFM long-range coupling [27] but can also be due to other factors like a canted AFM state of the system [27a, 27b]. The ZFC magnetizations of all the samples except for $x = 0.2$ show a drop in the magnetic moment, indicating AFM ordering in this system. As with other coexistence spin systems, the application of a magnetic field allows switching AFM domains to the FM state. The FC magnetization data, except for the composition $x = 0.4$, indicate that a small magnetic field of 50 Oe is enough to drive the AFM spin state to the FM state in NCSMO. The difference in the ZFC and FC magnetizations is found to decrease with an increase in the Ca concentration, which is evidence for an increase in canting of Mn^{3+} and Mn^{4+} moments with decrease in Ca concentration, favoring superexchange interactions between Mn–O–Mn. On lowering the temperature, ZFC magnetization of NCSMO 0.1 starts to increase at around 214 K and then undergoes a gradual drop down to 20 K. The gradual decrease in magnetic moment below T_C is due to the short range ordering of Mn^{3+} and Mn^{4+} which leads to AFM ordering. However, for NCSMO 0.3 and 0.4 in the region between T_C and T_N, magnetization remains constant which may be due to short-range FM ordering. The composition $x = 0.2$ does not show any drop in the magnetization; this might be due to the presence of more delocalized e_g electrons resulting in FM ordering. The inset of figure 4 shows the temperature dependence of $\delta M(T) = 2(M_{ZFC} - M_{FC})/(M_{ZFC} + M_{FC})$. All the compositions show a change in δM at a temperature which is above T_C and this temperature coincides with T^* (the temperature T^* will be discussed in the ESR section). This temperature region is attributed to the region in which magnetic phase separation occurs [27]. The phase transition is associated with the development of Jahn–Teller polarons and the partial real space ordering of Mn^{3+} and Mn^{4+} ions [28]. Moreover, all the compositions except for $x = 0.1$ show a strong deviation from the Curie–Weiss fit, which can be seen in the H/M versus T plot (figure 4). This deviation is
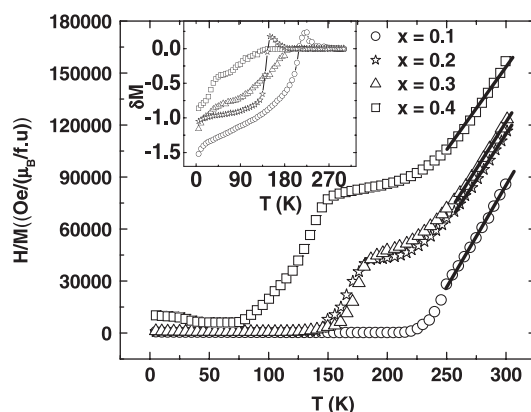
Figure 4. Curie–Weiss fit to susceptibility data of NCSMO. Inset: relative difference δM versus T plot.

a signature for the onset of short-range AFM interactions, which compete with ferromagnetic DE interactions in this temperature range. In analogy with half-doped manganites, the AFM interactions arise from real space ordering of Mn^{3+} and Mn^{4+} ions. However, due to the random distribution of A-site ions, the CO state is unstable and ferromagnetic DE prevails, which leads to the coexistence of AFM and FM phases in NCSMO [25]. A similar phenomenon is observed in half-doped $(Nd_{1-y}Sm_y)_{0.5}Sr_{0.5}MnO_3$ [29]. The effective magnetic moments, μ_{eff}, were calculated from the Curie–Weiss fit in the temperature region above 250 K and are given in table 2. The values are found to be larger than the spin only effective magnetic moment ($\mu_{eff} = 5.10 \ \mu_B$) of NCSMO, which reflects the evidence of magnetic polarons in the paramagnetic region [30]. The Jahn–Teller polarons due to Jahn–Teller distortion of Mn^{3+} ions affect the spin of the neighbors and become magnetic polarons, which in turn determine the transport as well as magnetic properties above T_C.

We carried out ESR studies to characterize the low temperature magnetic phenomenon. It is one of the probes for finding the existence of different magnetic phases and magnetic spin polarons. It has been reported that in manganites there is an anomalous behavior of the ESR linewidth as well as intensity due to the interplay of different exchange interactions between the magnetic ions. The spin Hamiltonian of the electron has contributions from Zeeman (H_Z), Heisenberg exchange (H_E), dipole–dipole (H_D), quadrupole–quadrupole (H_Q), antisymmetric exchange (H_{DM}) (Dzyaloshinsky–Moriya (DM) interaction) and crystal field interactions (H_{CF}) [14]. The spin moment arising from H_Z, H_D and H_Q does not have any significant effect in the phase transition regime but the effect of H_E, H_{DM} and H_{CF} is profound; this can clearly be seen in the linewidth as well as the intensity of the spectra of the manganites. The antisymmetric DM interactions H_{DM}, which arise from the tilting of the oxygen octahedra, favor superexchange interaction among the Mn ions [31]. H_{CF} is a second-order effective Hamiltonian due to the noncubic component of the crystal field interaction between a Mn ion and its oxygen neighbors.

The ESR spectrum of all samples is recorded in the temperature range from 300 to 100 K. When the temperature decreases, there is a shift of the center of the magnetic field and a narrowing of the line, both of which are clearly observable at the magnetic transition. In the paramagnetic region (PM), the ESR spectrum consists of a single line with a Lorentzian shape, but below the temperature T^* a new line appears and the lines are found to be broadened. It has been reported that there exist a short-range spin ordering between T^* and T_C or magnetic
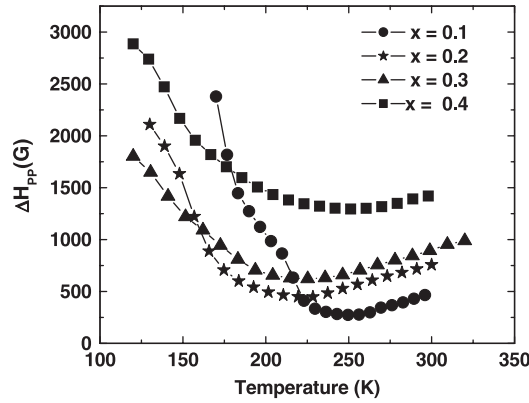
Figure 5. The temperature dependence of peak to peak linewidth ΔH_{PP} of the samples.

spin clusters [32]. The spectra have been fitted by using the derivative of the Lorentzian line shape of the form $\frac{dP}{dH} = \frac{d}{dH}[\frac{\Delta H}{(H-H_0)^2+\Delta H^2}]$, where P is the power absorbed by the sample from the transverse magnetic microwave field and keeping the resonance field H_0, the linewidth ΔH and the intensity of each line as adjustable parameters. Above T^* the ESR spectra could be fitted with a single absorption line. Below T^* the spectrum is found to be split into two Lorentzians (inset of figure 7(a)–(d)). The values of T^* and T_C are listed in table 2. The deviation of T^* from T_C is relatively small in NCSMO 0.1, which has the highest T_C. However, in the case of NCSMO 0.4 the value of T^* is much higher than T_C. This could be due to carrier localization at Mn sites. The T^* values match with the phase transition temperature (figure 4), which suggests that there is considerable coupling between lattice and magnetism in NCSMO. The temperature dependence of the peak to peak linewidth ΔH_{PP} is shown in figure 5. In the PM regime, the linewidth decreases linearly with decrease in temperature. The linear temperature dependence of ΔH_{PP} for $T > T_C$ is ascribed to the phonon modulation of the crystalline field [33]. As the temperature approaches T^* the linewidth goes through a minimum, and below T_C a rapid broadening is observed. The minimum near the transition is attributed to weak spin correlations due to different magnetic and structural phase transitions, which is significant for magnetically inhomogeneous samples [32]. Broadening of the linewidth below the transition temperature is due to the change in the spin–lattice interactions arising from the ordering of magnetic moments and heterospin interactions due the real space ordering of Mn^{3+} and Mn^{4+} ions [34]. In manganites, the temperature dependent anomalous behavior of the linewidth is due to the contributions from dipolar interaction, demagnetizing fields, crystal field effects and antisymmetric exchange interactions. However, the observed magnitude of the linewidth arising from the dipolar interaction and demagnetizing fields is negligible [35]. The temperature dependent narrowed linewidth in the manganites is due to anisotropic interactions as well as DM interactions. The crystal field effect and Jahn–Teller distortion cause the anisotropic interaction, while antisymmetric exchange terms arise from DM interactions $D_{ij}(S_i * S_j)$. DM interactions result in single-phonon absorption and emission, which cause spin flipping and thereby change in the exchange energy. DM interaction favors superexchange interaction between the ions [14]. The narrowest linewidth is obtained at a temperature of 250 K for both $x = 0.1$ and 0.4, which coincides with the T_C value of end members and 210 K and 225 K for $x = 0.2$ and 0.3, respectively. The broadening of linewidth is found to be greater in $x = 0.4$, due to heterospin dipolar interactions arising from the charge ordering of Mn ions reflected in the insulating AFM state of $x = 0.4$ [34]. The
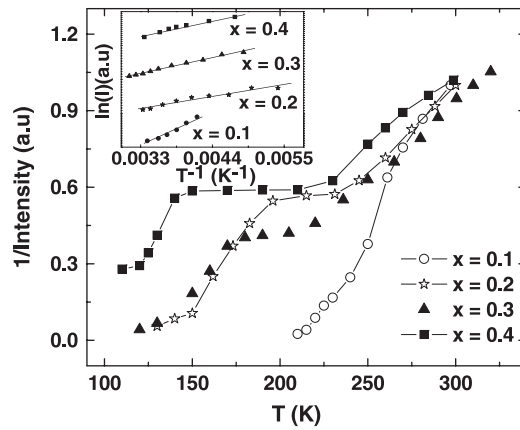
8

Figure 6. The temperature dependent ESR line intensity of NCSMO. Inset: ESR intensity fit to the Arrhenius equation.

temperature dependence of linewidth provides evidence for magnetic and structural transitions in the vicinity of T^*.

The temperature dependence of the ESR integrated intensity, I, is shown in figure 6. The intensity of the resonance signal is found to vary drastically with Ca doping. The intensity of the spectra at $T > T_C$ decreases with decrease of temperature and goes to a minimum at the magnetic transition for all samples. The temperature dependence of intensity in the paramagnetic region, $T > 250$ K, follows a Curie–Weiss law $I \propto \chi$. The intensity can be fitted to an Arrhenius equation of the form $I = I_0 e^{(\Delta E/k_B T)}$ where ΔE is the activation energy for dissociation of the paramagnetic spin clusters [37]. The inset of figure 6 shows plots of ln(intensity) versus inverse temperature for all the samples over the paramagnetic temperature range. The calculated values of ΔE (table 2) for NCSMO lie between 0.04 and 0.059 eV. They are less than the values found for NCMO ($\Delta E = 0.1$ eV) [36], NSMO (0.06 eV) [37] and ground state ferromagnetic metals ($\Delta E > 0.2$ eV) [13, 34]. The smaller values for the activation energy indicate the AFM correlations in NCSMO. The values of ΔE show that the Ca-rich and Sr-rich compositions of NCSMO have stronger intra-cluster interactions than those of the other compositions [13]. The ESR intensity deviates from the Curie–Weiss law, indicating that spin–lattice interaction is present in the vicinity of T_C which results in the formation Jahn–Teller polarons [30, 35]. This electron–phonon coupling or the Jahn–Teller coupling arises from real space ordering of Mn^{3+} and Mn^{4+} ions. This deviation can also be seen in χ_{DC} (figure 4), showing the correlation between temperature dependence of ESR intensity and dc magnetization. A similar phenomenon is observed in charge-ordered AFM systems like $Pr_{0.5}Ca_{0.5}MnO_3$ and coexisting FM–AFM systems like $(Nd_{1-y}Sm_y)_{0.5}Sr_{0.5}MnO_3$ [29]. By analogy to the above systems the up turn in the ESR intensity can be assigned to presence of AFM interactions in NCSMO.

The temperature dependence of the resonance center field is shown in figures 7(a)–(d). Below the temperature T^* the spectra of all the compositions split into two Lorentzians, which indicates the existence of two different magnetic phases in the samples [13]. The different magnetic resonances are due to spin moments having different relaxation rates in different crystallographic environments. One of the factors that affects the spin moment or the internal field is the exchange coupling constant (J_{ij}). The AFM coupling occurs at higher fields than FM coupling. Hence the lower (H_L) and higher field (H_H) resonances are attributed to FM
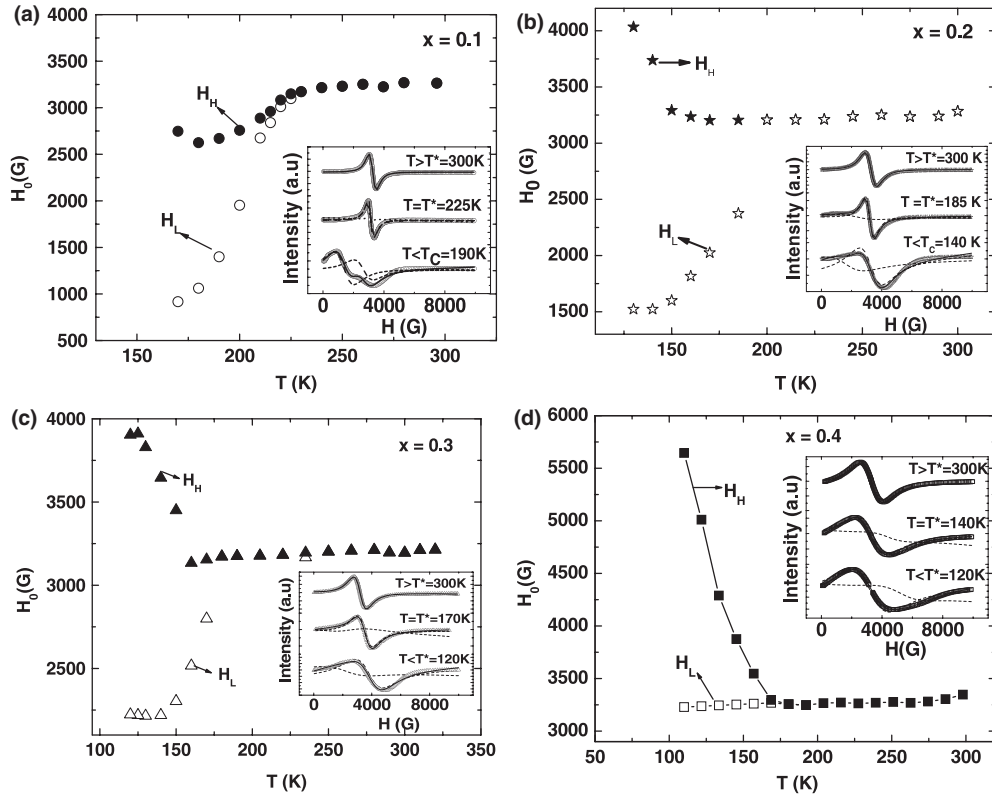
Figure 7. (a)–(d) The temperature dependence of the resonance center field (H_0) of NCSMO. Inset: ESR spectra with fitted (solid lines) and resolved curves (dotted lines) at various temperature ranges of the sample.

and AFM coupling, respectively, between the Mn ions [34, 37, 38]. In the temperature range T^* to T_C one of the coexisting phases is found to be paramagnetic for all compositions. As in NSMO, the temperature variation of the resonance fields of NCSMO with composition $x = 0.2$ and 0.3 reveals the presence of different coexisting phases such as PM–FM in the temperature range between T^* and T_C and FM–AFM below T_C. But for $x = 0.1$ and 0.4 the coexisting phases are PM–FM and PM–AFM, respectively, and we could not observe any FM–AFM phase in the temperature range 300–100 K. Hence for the Ca-rich composition, $x = 0.4$, the antiferromagnetic superexchange mechanism prevails, with the short-range DE interaction being responsible for the formation of the ferromagnetic phase which is in the transport as well as magnetization measurements. However, for the compositions $x = 0.1$, 0.2 and 0.3 the ferromagnetic metallic phase dominates, as can be seen in the magnetization measurements. The double exchange interaction between an inhomogeneous distribution of Mn^{3+} and Mn^{4+} leads to a ferromagnetic metallic state of the sample. The competition between superexchange induced short-range FM insulating or AFM and double exchange induced FM metallic states leads to the coexistence of phases in NCSMO [12].

4. Summary

The magnetotransport and ESR studies suggest the presence of coexisting phases in the NCSMO system. The coexisting phases in the 1:1 Mn^{3+}/Mn^{4+} system are ascribed to

the random distribution of A-site cations. There will be phases/regions corresponding to delocalized e_g electrons leading to FM phases and those regions with short-range ordering of Mn^{3+}/Mn^{4+} leading to AFM insulating phases. Competition between different exchange interactions leads to the coexistence of different phases in this system. Here, we have re-investigated a particular series of compounds which falls in the charge-ordered regime ($\langle r_A \rangle \sim$ 1.20 Å), where a FM metallic behavior was previously observed [17]. Our results clearly indicate that the compounds phase separate at low temperatures and the observed FM nature is a consequence of the phase separation phenomenon. Our results further indicate the importance of phase separation in the understanding of many complex phenomena in manganites. Further structural characterization using neutron diffraction is needed to elucidate the types of magnetic structure/interactions existing in the constituent phases observed at low temperatures.

Acknowledgments

References

[1]　Sen C, Alvarez G and Dagotto E 2007 *Phys. Rev. Lett.* **98** 127202
[2]　Salamon M B and Jaime M 2001 *Rev. Mod. Phys.* **73** 583
[3]　Woodward P M, Vogt T, Cox D E, Rao C N R and Cheetham A K 1999 *Chem. Mater.* **11** 3528
[4]　Tokura Y and Nagosa N 2000 *Science* **288** 462
[5]　Millange F, de Brion S and Chouteau G 2000 *Phys. Rev.* B **62** 5619
[6]　Maitra T and Taraphder A 2003 *Phys. Rev.* B **68** 174416
[7]　Zener C 1951 *Phys. Rev.* **181** 440
[8]　Ramirez A P 1997 *J. Phys.: Condens. Matter* **9** 8171
[9]　Xu Q Y, Wang R P and Zang Z 2005 *Phys. Rev.* B **71** 092401
[10]　Hwang H Y, Cheong S W, Radaelli P G, Marezio M and Batlog B 1995 *Phys. Rev. Lett.* **75** 914
[11]　Woodward P M, Vogt T, Cox D E, Arulraj A, Rao C N R, Karen P and Cheetham A K 1998 *Chem. Mater.* **10** 3652
[12]　Algarabel P A, De Teresa J M, Blasco J, Ibarra M R, Kapusta C, Sikora M, Zajac D, Riedi P C and Ritter C 2003 *Phys. Rev.* B **67** 134402
[13]　Shames A I, Rozenberg E, Gorodetsky G and Mukovskii Ya M 2003 *Phys. Rev.* B **68** 174402
[14]　Cooper B R and Keffer F 1962 *Phys. Rev. Lett.* **125** 896
[15]　Allodi G *et al* 1997 *Phys. Rev.* B **56** 6036
[16]　Papavassiliou G, Belesi M, Fardis M and Dimitropoulos C 2001 *Phys. Rev. Lett.* **87** 177204
[17]　Rao C N R, Santhosh P N, Singh R S and Arulraj A 1998 *J. Solid State Chem.* **135** 169
[18]　Damay F, Martin C, Maignan A and Raveau B 1997 *J. Appl. Phys.* **8** 6181
[19]　Pissas M and Papavassiliou G 2004 *J. Phys.: Condens. Matter* **16** 6527
[20]　Moritomo Y, Kuwahara H, Tomioka Y and Tokura Y 1997 *Phys. Rev.* B **55** 7549
[21]　Urushibara A, Moritomo Y, Arima T, Asamitsu A, Kido G and Tokura Y 1994 *Phys. Rev.* B **51** 14103
[22]　Lago J, Battle P D, Rosseinsky M J, Coldea A I and Singleton J 2003 *J. Phys.: Condens. Matter* **15** 6817
[23]　Jakob G, Westerburg W, Martin F and Adrian H 1998 *Phys. Rev.* B **58** 14966
[24]　Aruna S T, Muthuraman M and Patil K C 1999 *Solid State Ion.* **120** 275
[25]　Mahendiran R, Hervieu M, Maignan A, Martin C and Raveau B 2000 *Solid State Commun.* **114** 429
[26]　Nagaev E L 2001 *Phys. Rep.* **346** 387
[27a]　Ryzhov V A *et al* 2005 *Phys. Rev.* B **72** 134427
[27b]　Kawano H, Kajimoto R, Kubota M and Yoshizawa H 1996 *Phys. Rev.* B **53** 2202
[27c]　Lobanov M V *et al* 2000 *Phys. Rev.* B **61** 8941
[28]　Loudon J C, Mathur N D and Midgley P A 2002 *Nature* **420** 797
[29]　Kuwahara H, Moritomo Y, Tomioka Y, Asamitsu A, Kasai M, Kumai R and Tokura Y 1997 *Phys. Rev.* B **56** 9386

[30] Anil Kumar P S, Joy P A and Date S K 1998 *J. Phys.: Condens. Matter* **10** L269
[31] Choukroun J, Richard J L and Stepanov A 2001 *Phys. Rev. Lett.* **87** 127207
[32] Causa M T *et al* 1998 *Phys. Rev.* B **58** 3233
[33] Seehra M S, Ibrahim M M, Suresh Babu V and Srinivasan G 1996 *J. Phys.: Condens. Matter* **8** 11283
[34] Autret C, Gervais M, Gervais F, Raimboux N and Simon P 2004 *Solid State Sci.* **6** 815
[35] Sharma A, Sarangi S and Bhat S V 2006 *Phys. Rev.* B **73** 035129
[36] Janhavi P J, Gupta R, Sood A K and Bhat S V 2002 *Phys. Rev.* B **65** 024410
[37] Angappane S, Rangarajan G and Sethupathi K 2003 *J. Appl. Phys.* **93** 8334
[38] Autret-Lambert C, Gervais M, Gervais F, Simon P and Raimboux N 2005 *Solid State Sci.* **7** 1035
[39] Rodriguez-Martinez L M and Attfield J P 1999 *Phys. Rev.* B **59** 13539